*Desalination and Water Treatment*
www.deswater.com

doi:10.5004/dwt.2018.23174

156 (2019) 177–188
July

# Iron oxide modified polyethersulfone/cellulose acetate blend membrane for enhanced defluoridation application

C. Evangeline[a,e], V. Pragasam[a], K. Rambabu[b,*], S. Velu[b], P. Monash[b], G. Arthanareeswaran[c,*], Fawzi Banat[d]

[a]*Department of Bio-sciences, School of Biosciences and Technology, Vellore Institute of Technology, Vellore 632014, India, email: evangechriz@gmail.com (C. Evangeline), pragasam.v@vit.ac.in (V. Pragasam)*
[b]*Department of Chemical Engineering, School of Civil and Chemical Engineering, Vellore Institute of Technology, Vellore 632014, India, email: rambabu.k@vit.ac.in (K. Rambabu), svelu@vit.ac.in (S. Velu), monash.purushothaman@vit.ac.in (P. Monash)*
[c]*Department of Chemical Engineering, National Institute of Technology, Tiruchirappalli 620015, India, email: arathanareeg@gmail.com (G. Arthanareeswaran)*
[d]*Department of Chemical Engineering, Khalifa University of Science and Technology, The Petroleum Institute, Abu Dhabi, United Arab Emirates, email: fawzi.banat@ku.ac.ae (F. Banat)*
[e]*Department of Molecular biology and Genetics, School of Bioengineering and Biosciences, Lovely Professional University, Phagwara 144411, Punjab*

Received 10 June 2018; Accepted 20 September 2018

**ABSTRACT**

Fluoride removal in drinking water is usually performed through cost and energy intensive membrane techniques such as reverse osmosis, dialysis and electro-dialysis. Defluoridation using an effective and low cost ultra filtration membrane system is reported in this work. Iron (III) oxide ($Fe_2O_3$) nanoparticles modified polyethersulfone (PES)/cellulose acetate (CA) blend membranes were fabricated by phase inversion method. Composite membranes were prepared by incorporating incremental amounts of $Fe_2O_3$ nanoparticles. Synthesized membranes were analysed for morphological studies and ultra filtration characteristics. It was observed that the inclusion of iron oxide nanoparticles influenced the membrane structure resulting in enhanced ultra filtration properties. All of the iron oxide nanoparticles incorporated PES/CA membranes possessed increased hydrophilicity, porosity, water uptake and pure water flux as compared to pristine PES membrane. Membrane with 0.5 wt% $Fe_2O_3$ nanoparticles exhibited a maximum water flux of 156 L $m^{-2}$ $h^{-1}$. Fluoride removal performance confirmed the defluoridation potential of the $Fe_2O_3$ nanoparticles blended PES/CA membranes. Maximum fluoride removal efficiency of 70.3% was observed for a single ultra filtration run. SEM and AFM examinations showed the structural alterations in the composite membranes due to the nanoparticles addition. Reusability studies confirmed the enhanced durability of the blended membrane. Domestic application of the composite membrane was carried out by assessing its fluoride removal ability in natural water samples obtained from fluoride endemic area.

*Keywords:* Iron oxide; Polyethersulfone; Cellulose acetate; Defluoridation; Membrane

## 1. Introduction

Fluoride is a highly electronegative anion present in nature. It is present in the form of fluorides in various rocks such as fluorspar, fluorapatite, cryolite etc. Due to dissolution of fluoride containing rocks, fluoride ion gains access to water resources and contaminates them. Depending upon the fluoride concentration, it can be beneficial or hazardous for humans and is often regarded as "a double edged sword" [1]. Excessive intake of fluoride causes dental, skeletal and neu-

*Corresponding author.

*Presented at the InDA Conference 2018 (InDACON-2018), 20–21 April 2018, Tiruchirappalli, India*

rological disorders in humans [2]. Although there are several conventional technologies for fluoride removal, these methods possess several disadvantages such as pH dependence, leaching of the separation medium, high operational costs and require frequent regeneration [1,2]. As the conventional methods pose several drawbacks, an alternative methodology for efficient fluoride removal from aqueous stream is required.

Recent scientific advancements in chemical industries and increased effluent discharge have brought about a high need for concentration and separation. It has also lead to a great challenge for purification of chemical products, by-products, raw materials and other intermediates. Separation processes using membrane technology has gained prime importance with highly appreciable impact on chemical industries, pharmaceutical companies, energy storage, energy conversion and also in environmental protection [3].

Ultra filtration (UF) is considered as a promising membrane technique in various technical and industrial processes [4]. Due to its compact nature, easy fabrication, operational ease and less energy consumption, UF technology is preferred for separation and desalination applications on an industrial scale as compared to conventional filtration technologies [5]. The phenomenon of ultra filtration and its commercial significance have been widely studied by various researchers [4–9]. Polyethersulfone (PES) is widely used in the synthesis of ultra filtration membrane for treating water and wastewater [6,7]. Polyethersulfone is a highly stable polymer in terms of material characteristics [8,9] exhibiting splendid film forming and mechanical properties combined with excellent thermal, oxidative and hydrolytic strength [10,11]. Cellulose acetate (CA) membranes have good toughness and better fouling resistance as compared to PES and an appreciable desalting behavior [6]. The membrane properties and moderate durability of the CA based membranes reduce the need for frequent filter changes, thereby making them more cost effective [12]. However, a limitation of relatively lower flux has been reported for pure PES and pure CA membranes [9,13]. Therefore it has been suggested that modifying the membrane by blending with hydrophilic modifiers would result in membranes with higher flux and improved ultra filtration properties [13–17]. The modified blend membranes have the advantages of both hydrophilic as well as hydrophobic components. The modified membranes also possess enhanced ultra filtration characteristics (in terms of flux and rejection) and mechanical strength.

Development of polymeric UF composite membranes blended with inorganic nanoparticles is a recent trend in membrane research. Various polymeric materials and their blends play vital roles in selective separation of dissolved macromolecular particles [18,19]. These synergistic, hybrid blend materials exhibit unique optical, mechanical, thermal and electrical properties [20]. The enhancements in the physical properties of the membranes are due to the addition, dispersion and interaction of the nanoparticles with the polymer matrix [21,22]. Enhanced activity of the membrane is ascribed to the smaller particle size of the nanoparticles. Blending of the base polymer with various inorganic modifiers has produced composite UF membranes with enhanced properties in terms of flux, hydrophilicity, porosity and solute rejection [23,24].

Iron based nanoparticles are capable of providing enhanced hydrophilicity and also aid in enlargement of pores on the membrane [25]. Due to its high hydrophilicity, the drawback of low flux by pristine PES and CA membranes can be alleviated by employing iron oxide nanoparticles. Iron oxide also acts as an excellent and efficient sorbent of ionic contaminants from water sources, in addition to increase in mechanical stability of the membrane [26]. Contaminant metal ions were removed by membranes modified with iron oxide nanoparticles which enhance its performance when compared to other metal oxide impregnated membranes [27–31]. Iron oxides in nano forms have unique properties such that the nanoparticles can be modified or coupled with functional groups desirable for exhibiting new properties [29,32].

On analyzing the various results of previous investigations, it can be inferred that the iron (III) oxide ($Fe_2O_3$) nanoparticles modified PES/CA blend membranes could be capable of trapping fluoride ions from the feed fluoride solution [33,34]. The current work is an attempt to increase the flux of the PES based UF membrane as well as its fluoride removal ability by enhancing the hydrophilicity of the pure PES and CA membranes. The synthesized membranes were characterized by scanning electron microscopy, atomic force microscopy and ultra filtration characterizations such as membrane hydraulic resistance, water uptake study, pure water flux and finally for the fluoride removal efficacy. Additionally unspiked real water samples and those that were spiked with fluoride ions were subjected to ultra filtration to study the fluoride removal ability of the blend membrane with better ultra filtration characteristics. The re-usability of the best blend membrane was also analyzed and the obtained results are discussed.

## 2. Materials and methods

### 2.1. Chemicals and reagents

Ferrous chloride ($FeCl_2$) and 25% ammonia solution were procured from Sisco Research Laboratories (Mumbai, India). Polyethersulfone (PES, $M_W$ = 58000 g $mol^{-1}$) polymer was acquired from Solvay Specialities, India. Cellulose acetate polymer was purchased from Loba chemie, Mumbai, India. *N, N*-dimethyl formamide (DMF) was obtained from Fischer Scientific, India. Sodium hydroxide and sodium fluoride was purchased from Rankem Ltd, India. Demineralized water was used as the gelation medium for membrane synthesis. All other chemicals used for the membrane development process were of analytic grade.

### 2.2. Iron oxide nanoparticle synthesis

$Fe_2O_3$ nanoparticles used in this work were prepared by a chemical co-precipitation technique as explained elsewhere [35]. Briefly, iron oxide nanoparticles were synthesized by the modified co-precipitation method by adding 0.7 mol $L^{-1}$ ammonia solution to 1% ferric chloride solution at 80°C. The obtained black precipitate was washed thoroughly with water, until neutral pH and freeze dried to get the nanoparticles. The synthesized and characterized nanoparticles were further processed to be blended within PES/CA blend.

### 2.3. Membrane development

Phase inversion technique was employed in the development of asymmetric membranes predominantly those using

polyethersulfone and/or cellulose acetate as starting materials [36,37]. The cast solution composition for the various membranes synthesis is shown in Table 1. For instance, M5 membrane dope of 25 g was prepared by dissolving 4.5 g of PES (18 wt%), 0.5 g of CA (2 wt%) and 0.5 g of $Fe_2O_3$(2 wt%) in 19.5 g of DMF solvent (78 wt%). The casting solution was mechanically stirred for 4 h at 300 rpm at a temperature of 60°C, to attain homogeneity. The cast solution was then cooled to 20°C and allowed to stand for 2 h to remove air bubbles. The mixture was then cast onto a smooth glass plate with a film applicator to a thickness of 250 microns and immediately immersed into a gelation bath of pure distilled water at 10°C [38]. The prepared membranes were taken out of the gelation bath after an hour and completely washed with distilled water to remove residual solvent traces from the membrane. The membranes were then kept in distilled water for another 24 h to ensure complete phase separation. Different compositions of the blend membrane were developed by adopting the same procedure. All the developed membranes were stored in distilled water until further use [39].

### 2.4. Scanning electron microscopy

The surface and cross section morphology of the $Fe_2O_3$ nanoparticles included and excluded membrane samples were studied using scanning electron microscopy analysis (Quanta FEG 200, FEI Co., USA). Representative membranes samples of each concentration of $Fe_2O_3$ nanoparticles were cut into small pieces and blot dried with filter paper. The pieces were immersed in liquid nitrogen for 20–30 s until frozen and were fractured into smaller pieces and stored in desiccators. The cross section and top surface view of these membranes were subjected to SEM analysis.

### 2.5. Atomic force microscopy

Samples from each composition of prepared membrane series were subjected to atomic force microscopy (SPM CP-II, Veeco Co., USA) to measure the roughness of the membrane surface and pore characteristics. The images taken by scanning over the membrane surface with a sharp tip represents the topography of the membranes in 3D. These topographic images were used to study the structural differences in the blend membranes developed for fluoride removal from water.

Table 1
Composition of unmodified and $Fe_2O_3$ nanoparticles modified PES/CA blend membranes

| Membrane ID | PES (wt %) | CA (wt %) | $Fe_2O_3$ nanoparticles (wt %) | Dimethyl formamide (wt %) |
|---|---|---|---|---|
| M0 | 18 | 0 | 0 | 82 |
| M1 | 18 | 2 | 0 | 80 |
| M2 | 18 | 2 | 0.1 | 79.9 |
| M3 | 18 | 2 | 0.5 | 79.5 |
| M4 | 18 | 2 | 1 | 79 |
| M5 | 18 | 2 | 2 | 78 |

### 2.6. Infrared Spectroscopy

Surface chemistry of the $Fe_2O_3$ nanoparticles and the prepared composite membranes was analyzed through Infrared spectroscopy in a Fourier Transform Infrared (FTIR) spectrometer (Perkin Elmer–System One, USA). The spectra were obtained in a region of 4000–400 $cm^{-1}$. The spectra obtained were obtained at a resolution of 2 $cm^{-1}$ and were baseline corrected in the entire region of the spectra.

### 2.7. Ultra filtration set up

Ultra filtration experiments were performed in a stirred type, dead end filtration cell with a capacity of 450 ml. The schematic representation of the set-up is shown in Fig. 1. The diameter of the membrane that could be studied was 7.6 cm and the effective area of filtration was 45.6 $cm^2$. Inert nitrogen gas was used as the pressure source. The compaction pressure for the apparatus was 313 kPa and flux pressures were 147, 196, 245 and 294 kPa.

### 2.8. Membrane characterization

#### 2.8.1. Water uptake and porosity

Water uptake capacity of a membrane is considered to be a very important parameter for membrane characterization studies. Membrane samples were cut to 2 × 2 cm size and soaked in water for 24 h and their weight was noted immediately after blotting the membranes. These wet membranes were dried at 105°C for 12 h and the dry weight was noted. The water uptake (*WU*) capacities of the membranes were calculated using Eq. (1) [40].

$$WU = \frac{W_w - W_d}{W_w} \times 100 \quad (1)$$

where *WU* is water uptake (%), $W_d$ (kg) and $W_w$ (kg) are dry and wet weight of the blend membrane samples, respectively.

Porosity of the prepared membranes was calculated by dry-wet weight method in which the wet weight and dry weight of the respective sample was observed. Membrane porosity (ε) was calculated using Eq. (2) [41].

$$\varepsilon = \frac{W_w - W_d}{\rho_w V_m} \times 100 \quad (2)$$

where $V_m$ ($m^3$) is membrane volume and $\rho_w$ (kg $m^{-3}$) is water density. The measurement process was repeated for three times and the average values have been reported.

#### 2.8.2. Pure water flux

The water flux of the membrane is the parameter that determines the rate at which the pure water passes through the membrane. Membrane samples were cut into circular discs of 7.6 cm diameter and were placed inside the ultra filtration batch cell whose capacity is 450 ml. Nitrogen gas was used to create the required pressure to force water through the membrane. The membranes were compacted prior to flux measurement at a higher pressure of 313 kPa

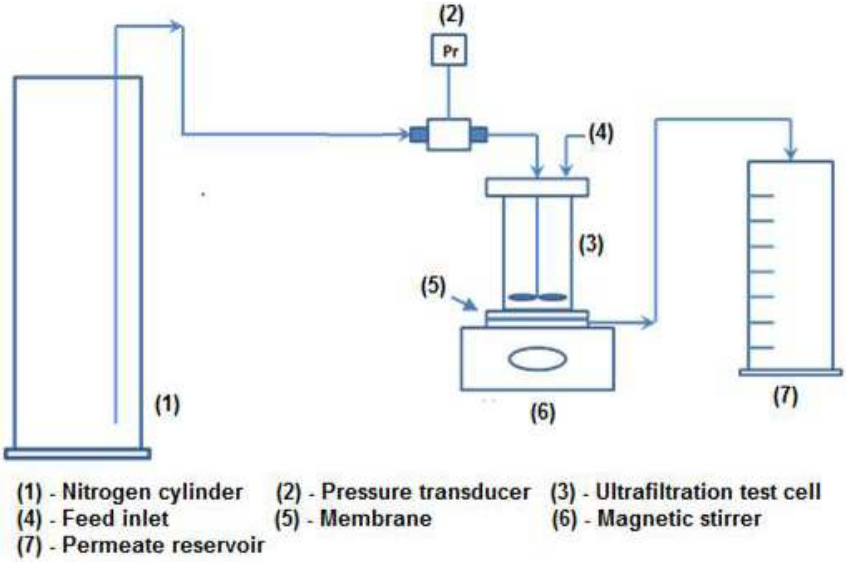


Fig. 1. Schematic diagram of the dead-end filtration system.

for five batch cycles to ensure steady state flux. Following compaction, the membranes were subjected to water flux analysis at different pressures of 147, 196, 245 and 294 kPa. Fixed amount of permeate samples were collected under steady state flow and the time taken for sample collection was noted. The pure water flux ($J_w$) of each membrane was calculated using Eq. (3) [40,41].

$$J_w = \frac{Q}{A\Delta t} \tag{3}$$

where $J_w$ is the pure water flux (L m$^{-2}$ h$^{-1}$), $Q$ is the quantity of permeate (L), $A$ is membrane area(m$^2$) and $\Delta t$ is the permeate collection time (h).

*2.8.3. Membrane hydraulic resistance*

Hydraulic resistance of a given membrane was determined through a plot between pure water flux and applied pressures. The hydraulic resistance for a given membrane was obtained from the inverse of the slope between the pure water flux ($J_w$) and trans-membrane pressure difference ($\Delta P$) of the respective membrane [14].

*2.8.4. Average pore size*

Average pore radius ($r_m$) of the prepared membranes was determined using Guerout–Elford–Ferry equation as given in Eq. (4) based on filtration velocity method [8,41].

$$r_m = \sqrt{\frac{(2.9-1.75\varepsilon)\times 8\eta_w l q}{\varepsilon \times A \times \Delta P}} \tag{4}$$

where ε is the membrane porosity, $\eta_w$ is the dynamic viscosity of water (Pa s), $l$ is the membrane thickness (m), $q$ is the volume of the water permeated per unit time (m$^3$/s), $A$ is the effective area of the membrane (m$^2$), and $\Delta P$ is the trans-membrane pressure (MPa).

*2.8.5. No. of pores*

The number of pores per unit surface area ($n$) in the membrane was determined using Sarbolouki equation (based on Poiseuille's law) as given by Eq. (5) [5].

$$n = \frac{\varepsilon}{\pi r_m^{\,2}} \tag{5}$$

where $n$ is the number of pores per unit surface area (m$^{-2}$), ε is the porosity and $r_m$ (m) is the average radius of the pores.

*2.8.6. Surface hydrophilicity*

The hydrophilic ability of the prepared membranes was determined by measuring their static contact angle with water droplets through a goniometer (DGX Digidrop, France). For this purpose, pure water droplets were placed on the outer membrane surface using a micro-syringe at several random positions and the water contact angle with the membrane surface was measured by imaging the droplets using a digital microscope. To minimize the measurement errors, average contact angle values are reported.

*2.9. Fluoride removal studies*

The stock solution of fluoride was prepared by dissolving 1 g of sodium fluoride in 1000 ml of double distilled water. Working solutions were diluted from the stock fluoride solutions. Fluoride ion removal studies were carried out by ultra filtration using the dead end UF stir cell at an applied pressure of 294 kPa. Sample of permeate stream for each membrane was collected separately in graduated tubes. The fluoride concentrations in the permeate samples were analyzed using fluoride ion selective electrode (EUTECH-Thermo Scientific Pvt. Ltd.). Fluoride removal (*% FR*) was calculated by Eq. (6).

$$\%FR = \left(1 - \frac{C_p}{C_f}\right) \times 100 \tag{6}$$

where $C_p$ and $C_f$ are the fluoride concentrations (g $L^{-1}$) in the permeate and feed streams, respectively.

### 2.10. Membrane re-usability studies

The membrane with the best fluoride removal performance was selected to study its re-usability in fluoride removal. 1% sodium hydroxide was used as the desorbing agent to remove fluoride ions from the membrane. After each batch run, the membrane was immersed in fresh NaOH solution for 30 min. The membrane was then washed thoroughly with excess of deionized water and the fluoride removal test was carried out sequentially for further cycles.

### 2.11. Application on real water samples

Water collection bottles of volume 500 ml were washed thoroughly with distilled water and dried. These were used to collect real water samples from ground water sources in Ranipet, Ambur and Vaniyambadi areas of Vellore district in Tamil Nadu, India. The real water samples were subjected to ultra filtration using the membrane with maximum fluoride removal. The procedure was same as described for in-house fluoride removal studies. The initial and final fluoride concentrations were estimated using fluoride ion selective electrode with a lowest fluoride detection limit of 0.02 mg $L^{-1}$. Unspiked real water samples and those which were spiked with 20 mg $L^{-1}$ of fluoride ions were subjected to ultra filtration studies using the dead end UF stirred cell to estimate the amount of fluoride ions removed by the membrane.

## 3. Results

### 3.1. Scanning electron microscopy

The top surface and cross-sectional view of the unmodified PES, PES/CA blend and $Fe_2O_3$ nanoparticles modified PES/CA blend membranes are presented in Figs.2 and 3. From the SEM micro graphs, the dense and smooth nature of the virgin membranes can be observed as matched against the $Fe_2O_3$ nanoparticles blend membranes. It was also inferred that the amount of iron oxide nanoparticles added to the cast solution influenced the pore morphology for the resulting membrane. Formation of skin layer is in accor-

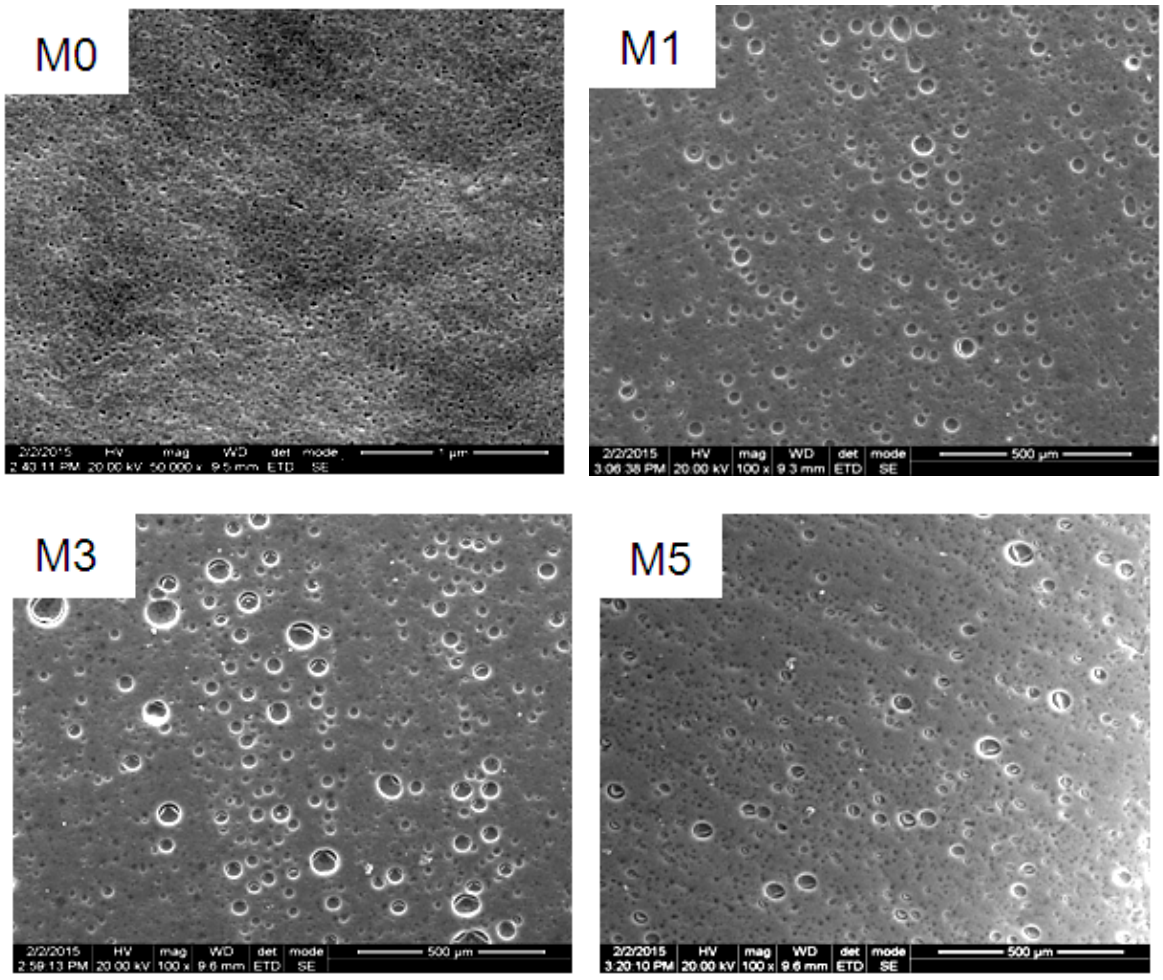


Fig. 2. Surface SEM images of the prepared pure and blend membranes.

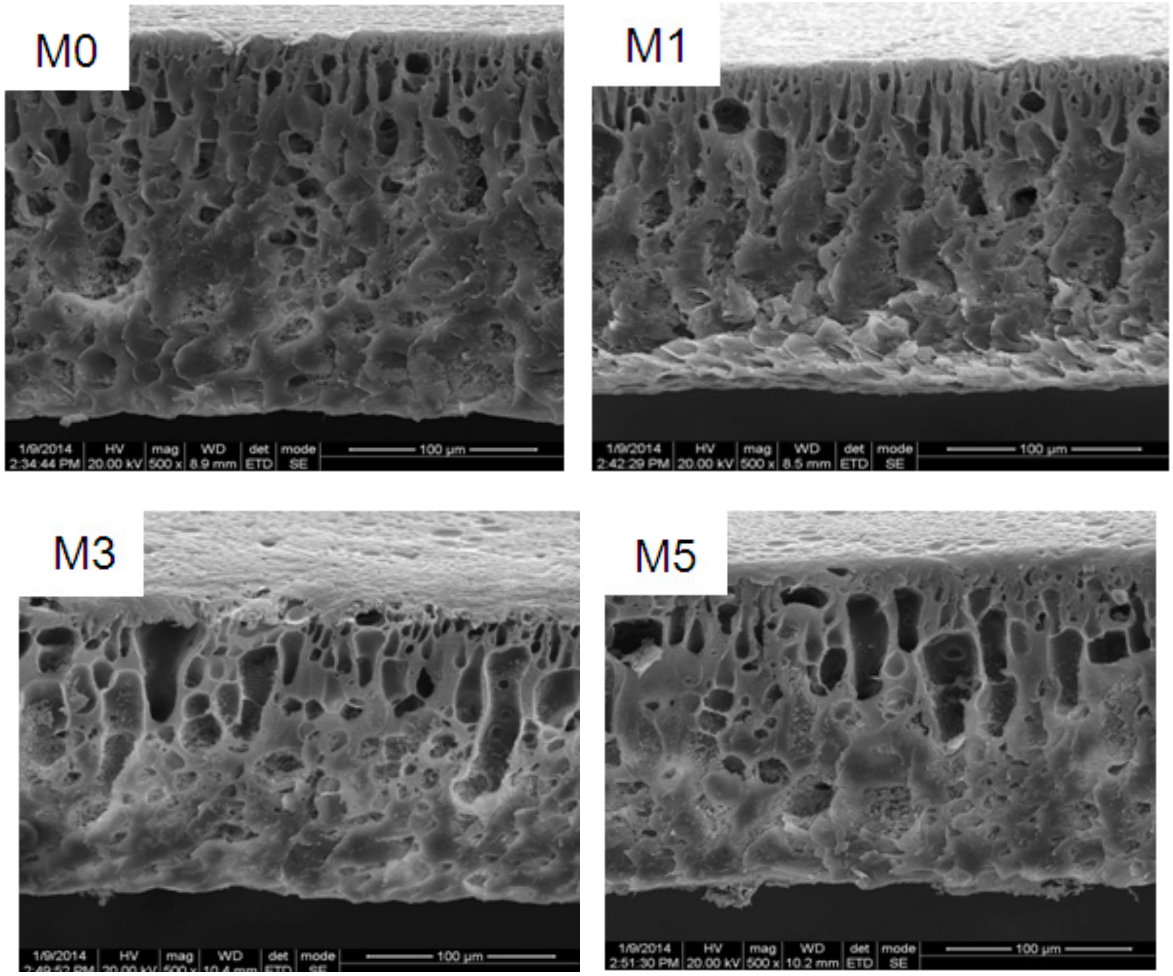


Fig. 3. Cross-section SEM images of the prepared pure and blend membranes.

dance with spinodal decomposition mechanism. Increase in $Fe_2O_3$ nanoparticles concentration with decreased amount of DMF solvent, weakened the affinity between solvent and non-solvent which resulted in more porous skin layer. From the top surface view (Fig. 2), it could be seen that the surface pores for M3 membrane (0.5 wt% $Fe_2O_3$ nanoparticles) were enlarged as compared to pure PES membrane. This observation can be used to describe the uniform dispersion of the nanoparticles throughout the surface and their preferential leaching during the phase inversion process, resulting in larger size pores. The spurted nanoparticles caused lower continuity in the membrane surface and thereby resulted in homogenous surface of increased pore size. Membrane with enlarged pore size has high permeate flux potentials through them [29].

However, the pore size got constricted with further inclusion of iron oxide nanoparticles as seen in M5 membrane (2 wt% $Fe_2O_3$ nanoparticles). The reduction in pore size was due to facial pore congestion of the accumulated $Fe_2O_3$ nanoparticles present very near to top layer. In general, the viscosity of the membrane dope solution was increased with the addition of nanoparticles, resulting in delayed demixing [41]. Migration of the iron oxide nanoparticles to the secondary solvent through the interface surface was hindered due to the delayed mixing rate. This caused the accrual of nanoparticles near the surface pore and hence in reduced surface pore size.

Fig. 3 shows the cross sectional view of the prepared membranes. Sub-layer formation is in good agreement with nucleation and growth mechanism. Pure PES membrane (M0) possessed a spongy and less inter-connected support layer. Inclusion of iron oxide nanoparticles resulted with membranes with more fingers like sublayer. This can be ascribed to the hydrophilic effects of inorganic $Fe_2O_3$ nanoparticles. Inclusion of the hydrophilic $Fe_2O_3$ nanoparticles increased the non-solvent diffusion rate into the film resulting in the formation of voided sublayer. Membranes with well-connected sublayer have a high flux through them [42]. In case of M3 membrane, the finger like structures run almost uniformly while in case of M5 membrane dead end structures could be observed. This can be explained by the dominant viscous effect of nanoparticles addition surpassing its hydrophilic effect after a critical concentration of 0.5 wt% [43,44]. These observations indicate the possibility of high flux associated with M3 membrane than M5 membrane. Moreover, the thickness of the top-layer for M5 membrane was substantial as compared to M3 membrane which would hin-

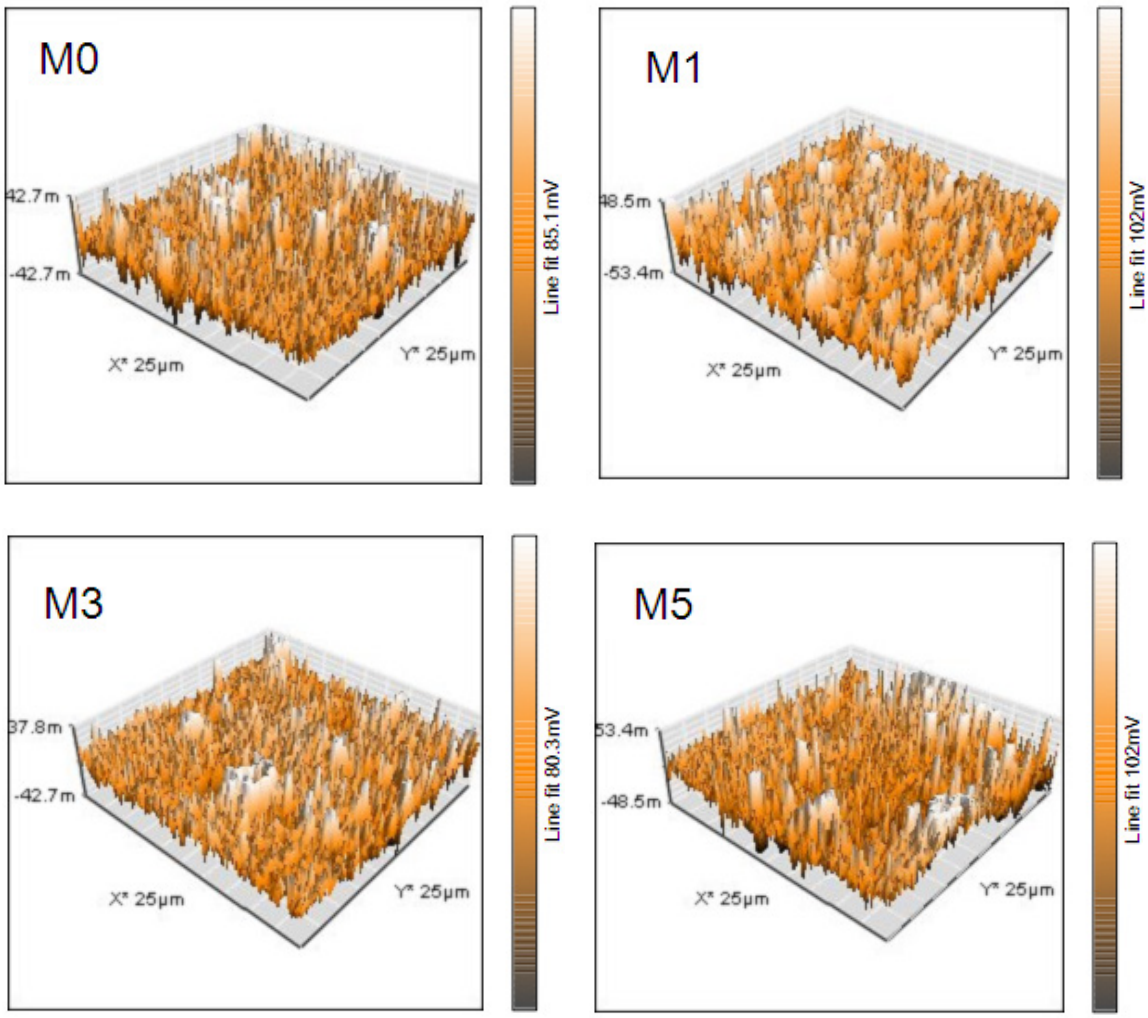


Fig. 4. Topographic AFM images of the prepared membranes.

der the permeate flux through M5 membrane, in spite of its porous sublayer [29].

### 3.2. Atomic force microscopy

The atomic force microscopy of PES, CA and $Fe_2O_3$ nanoparticles blend membranes were imaged and are shown in Fig. 4. A view angle of 45°C was fixed in order to appreciate the three dimensional pattern of the AFM images for an effective area 25 µm × 25 µm. Pores on the surface of the membranes may be identified as the areas in dark or depressions, while the bulges indicate the bright regions. High variations on the surface and pore size would result in high surface roughness of membranes [43]. The measured surface roughness for the synthesized membranes is presented in Table 2. It was seen that the surface roughness for iron oxide nanoparticles incorporated membranes increased up to 0.5 wt% of the nanoparticle concentration. Increase in surface roughness was due to the uniform dispersion of nanoparticles on the surface and enlarged surface pore size [30]. Membranes with higher concentration of $Fe_2O_3$ nanoparticles (> 0.5 wt%) showed a decrease in their surface roughness. This can be explained again by the low concentration of $Fe_2O_3$ nanoparticles on the membrane surface. Higher content of the nanoparticles resulted in larger hunks which would have deposited on the cross section than the membrane surface. The reduced pore size of the M4 and M5 membrane was also responsible for the reduced surface roughness of these membranes.

Table 2
Surface roughness of the prepared membranes

| Membrane ID | Surface roughness (nm) |
|---|---|
| M0 | 33.33 |
| M1 | 47.80 |
| M2 | 155.63 |
| M3 | 192.78 |
| M4 | 101.66 |
| M5 | 79.78 |

### 3.3. Fourier Transform Infrared Spectroscopy

FTIR analysis was performed for the $Fe_2O_3$ nanoparticles and M3 composite membrane to understand the various functional groups in the samples and also the interaction of the nanoparticles with the polymer matrix. The obtained spectra are presented in Fig. 5. For the nanoparticles, the peak seen at 1431 $cm^{-1}$ is attributed to the stretching vibrations of C=O group and the peak at 462 $cm^{-1}$ is assigned to the Fe–O group [45]. In case of the M3 membrane, the vibrational stretch felt around 3240 $cm^{-1}$ is ascribed to the –OH bond due to water absorption of the included nanoparticles. The peaks at 1650 and 1578 $cm^{-1}$ represented the characteristic aromatic bands of the PES structure while the sharp spectra at 1153 $cm^{-1}$ was due to the symmetric vibration of the $SO_2$ group. The vibrational effects of acetate group in CA were inferred through the absorption peak at1749 $cm^{-1}$. The characteristic spectra felt at 465 $cm^{-1}$ for the M3 membrane confirms the successful binding of the $Fe_2O_3$ nanoparticles with the PES/CA polymer matrix. FTIR studies confirmed the homogeneity of the PES/CA polymer blending and the successful binding of $Fe_2O_3$ nanoparticles in the membrane.

### 3.4. Membrane characterization

#### 3.4.1. Water uptake

Water uptake capacity of a membrane is an indirect indication of its flux behavior and hydrophilicity [14]. All the prepared membranes were thoroughly soaked with distilled water and the water content of the membranes was estimated. Water uptake of the $Fe_2O_3$ nanoparticles modified PES/CA blend membranes was found to be higher than the unmodified PES and PES/CA membranes. As illustrated in Table 3, it was observed that the water uptake capacity increased with the increase in $Fe_2O_3$ nanoparticles in the blend membranes. Membrane M2 and membrane M5 with the least and the highest concentration of $Fe_2O_3$ nanoparticles exhibited 67.62% and 74.27% of water uptake. The increase in water uptake could be explained by the availability of large pore volume due to the modifier action. Also, the hydrophilic nature of the iron oxide nanoparticles entrapped in the membrane matrix caused an increase in water uptake of the blend membranes.

#### 3.4.2. Pure water flux

Fig. 6 shows the permeate water flux variation with applied pressure for all of the prepared membranes. The

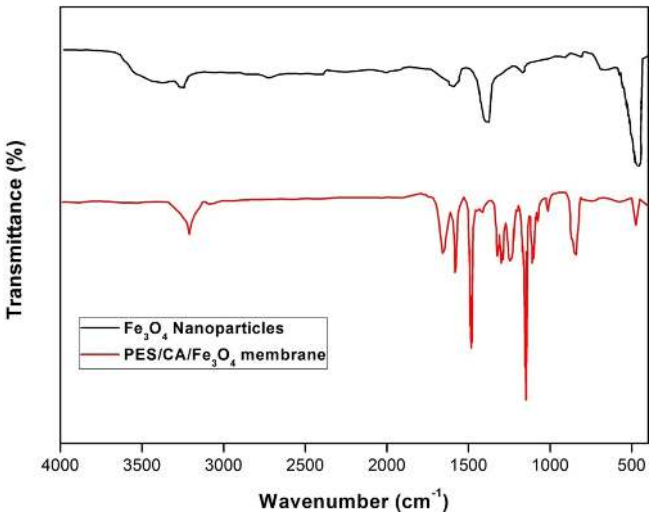


Fig. 5. FTIR spectra of the $Fe_2O_3$ nanoparticles and PES/CA/$Fe_2O_3$ membrane.

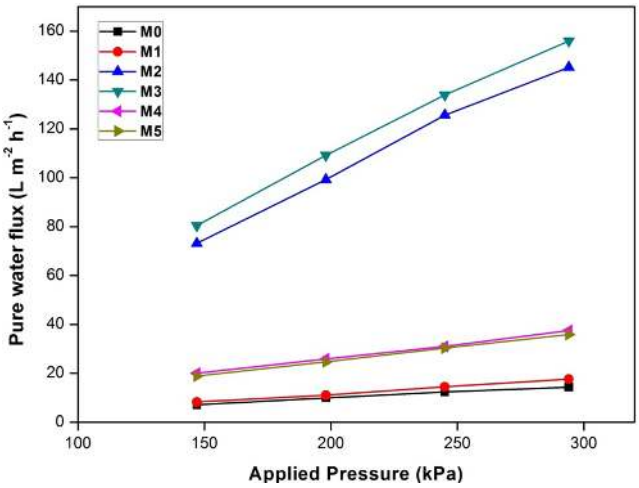


Fig. 6. Pure water flux of $Fe_2O_3$ nanoparticles modified PES/CA blend membranes and virgin membranes at various pressures.

Table 3
Ultrafiltration characteristics of unmodified and $Fe_2O_3$ nanoparticles modified PES/CA blend membranes

| Membrane ID | Water uptake (%) | Membrane resistance (Pa s $m^{-1}$) × $10^{10}$ | Porosity (ε) | Average pore radius (nm) | No. of pores ($m^{-2}$) × $10^{11}$ | Contact angle (degree) |
|---|---|---|---|---|---|---|
| M0 | 58.49 | 7.35 | 0.192 | 33.1 | 5.2 | 68.42 |
| M1 | 61.26 | 6.15 | 0.225 | 34.3 | 6.17 | 62.71 |
| M2 | 67.62 | 0.72 | 0.277 | 88.2 | 1.13 | 54.92 |
| M3 | 72.46 | 0.67 | 0.301 | 86.1 | 1.32 | 48.06 |
| M4 | 73.81 | 2.8 | 0.31 | 41.7 | 5.66 | 43.73 |
| M5 | 74.27 | 2.91 | 0.317 | 40.4 | 6.19 | 39.87 |

water flux of PES/CA blend membranes modified with $Fe_2O_3$ nanoparticles was found to be better than the pure PES and the unmodified PES/CA blend membrane. An increasing pattern of permeate water flux was observed with increase in the concentration of the $Fe_2O_3$ nanoparticle upto 0.5 wt%. This can be explained by the presence of finger like support layer in the membrane as revealed by the SEM micro graphs [11,37]. However, the water flux decreased for PES/CA blend membranes with more than 0.5 wt% $Fe_2O_3$ nanoparticles. Collapse of the support layer and the densification of the top layer caused the decreased water flux for these membranes. Membrane M3 exhibited a maximum water flux of 156 L $m^{-2}$ $h^{-1}$ at an applied pressure of 294 kPa, as compared to all other membranes. This was about ten times higher than that of the pure PES and unmodified PES/CA blend membrane. Results obtained for pure water flux were in accordance with the SEM interpretations of prepared membranes.

### 3.4.3. Membrane resistance

The resistance of the membrane denotes the intrinsic resistance or tolerance offered by the membrane for the passage of pure water at an applied hydraulic pressure. The membrane hydraulic resistance for all of the synthesized membranes is presented in Table 3. From the experimental studies, it was evident that the intrinsic resistances of $Fe_2O_3$ nanoparticles blend membranes were comparatively lesser, enabling high water fluxes through them. The lowest membrane resistance value of $0.67 \times 10^{10}$ Pa s $m^{-1}$ was observed for M3 membrane (0.5 wt% nanoparticles) due to its well-connected porous sublayer as compared to other membranes. Pure water flux and membrane resistance analysis clearly indicated the enhancement in mass transport due to $Fe_2O_3$ nanoparticles addition to PES/CA blend system.

### 3.4.4. Porosity, average pore size and number of pores

Porosity measurement results for prepared membranes are presented in Table 3. It could be seen that porosity of the developed membranes increased with increasing amounts of iron oxide nanoparticles. The interaction between solvent molecules and polymer was declined by the blockage offered by the $Fe_2O_3$ nanoparticles [46]. This resulted in easy diffusion of the solvent molecules from the matrix to the gelation bath, thereby enhancing the porosity. It was also observed that the porosity of the membranes had a faster incremental rate up to 0.5 wt% concentration of $Fe_2O_3$ nanoparticles and thereafter a much sluggish rate. This was due to agglomeration of $Fe_2O_3$ nanoparticles within the walls of the pores than on the membrane surface, for higher levels of $Fe_2O_3$ nanoparticles.

Membrane throughput highly depends on the size and number of pores being formed in the membranes. Average pore radius ($r_m$) and number of pores ($n$) were calculated using Eqs. (4) and(5) through pure water studies and the results are tabulated in Table 3. Pristine PES and unmodified PES/CA blend membranes showed characteristic low pore sizes of about 33.1 nm and 34.3 nm. Membranes M2 and M3 exhibited a comparatively larger pore size of 88.2 nm and 86.1 nm among the synthesized series. The larger pore sizes could be ascribed to the preferential leaching of the $Fe_2O_3$ nanoparticles from the membrane surface during membrane formation. A decreased pore size for M4 and M5 membrane was due to dominant accumulation of the nanoparticles on the membrane wall than the top surface. This was seen as an indication of non-uniform distribution of the $Fe_2O_3$ nanoparticles in these membrane matrixes. Surface pore densities were high for the unmodified PES and PES/CA blend membranes owing to their smaller pore size. Results obtained for average pore size and number of pores studies were in accordance with SEM and AFM observations.

### 3.4.5. Surface hydrophilicity

The hydrophilicity of the membrane determines the permeability and the hydraulic resistance offered by the membrane for free flow of water across it [24]. Surface hydrophilicity is assessed by measuring the static contact angle of the membranes. The hydrophilicity of the membrane surface is higher when the contact angles are smaller [44]. From Table 3, it could be seen that an increase in weight percentage of the $Fe_2O_3$ nanoparticles decreased the contact angle of the membranes.It was inferred that the addition of iron oxide nanoparticles increased the hydrophilicity of the composite membranes. Hydrophilicity enhancement was attributed to the abundance availability of active sites on the inorganic iron oxide nanoparticles for the attachment of polar functional groups [24]. Increase in hydrophilic nature of the membrane is also connected to the fouling resistance of the membrane [41]. Thus the $Fe_2O_3$ nanoparticles modified PES/CA blend membranes were expected to have comparatively good antifouling abilities.

### 3.4.6. Fluoride removal

Fluoride ion removal studies were carried out by ultra filtration using the dead end UF stirred cell for an applied pressure of 294 kPa. Fluoride feed solutions were prepared by diluting the stock solution of concentration 1000 mg $L^{-1}$. The permeate solution samples of the corresponding membranes were collected separately in graduated tubes. The fluoride removal efficiency was estimated by Eq. (6) and the obtained results are plotted in Fig. 7. Fluoride removal percentage increased with an increase in the $Fe_2O_3$ nanoparticles concentration until 0.5 % (Membrane M3), and decreased with further increasing concentrations. The better rejection of M3 membrane is because of the efficient dispersion of the $Fe_2O_3$ nanoparticles providing more active sites for fluoride ion adsorption. The low rejection of M4 and M5 membranes clearly indicated the decreased effect of $Fe_2O_3$ nanoparticles due to agglomeration effects.

Through the fluoride removal studies, it was concluded that the adsorption was the dominant mode of fluoride ion removal, in which the amount and dispersion of the $Fe_2O_3$ nanoparticles played a critical role for the membrane performance. Increased amount of iron oxide nanoparticles in M4 and M5 membranes caused more defects and more heterogeneity in the membranes. Agglomerated nanoparticles of M4 and M5 membranes decreased the available surface area for the fluoride adsorption resulting in low fluoride removal efficiency as compared to M3 membrane. Membrane M3 which offered the maximum pure water flux owing to increased

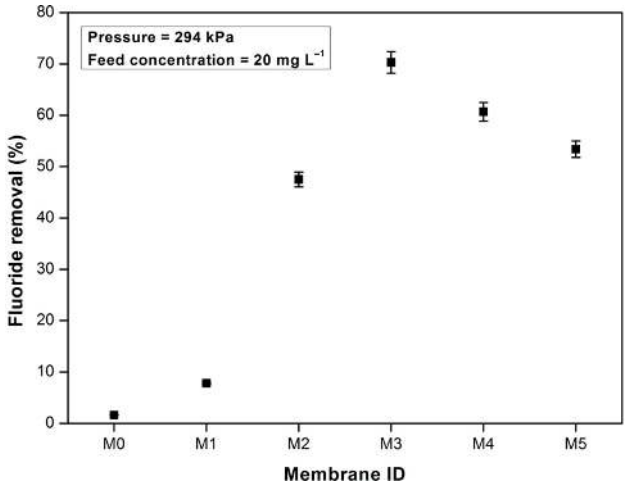


Fig. 7. Fluoride removal performance by unmodified and $Fe_2O_3$ nanoparticles modified membranes.

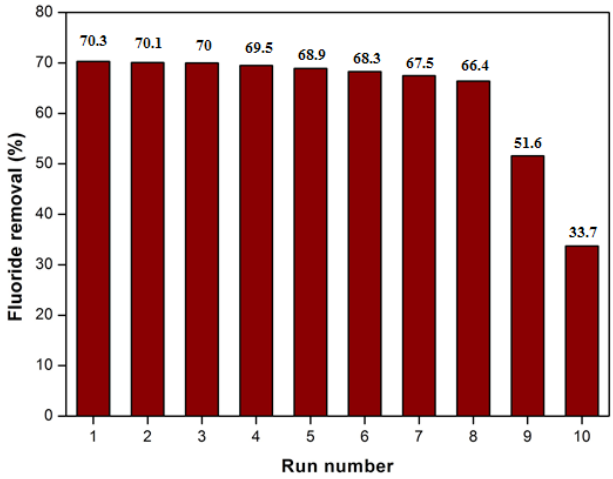


Fig. 8. Re-usability of PES/CA/$Fe_2O_3$ membrane for ten sequential runs.

porosity and hydrophilicity, also offered the maximum fluoride removal of 70.3% for the prepared membrane series. It was also noted that the fluoride removal efficiency for all iron oxide nanoparticles modified membranes was higher than the virgin PES and unmodified PES/CA blend membranes.

Considering the ultra filtration characteristics especially the pure water flux, fluoride rejection and the morphological features, it was evident that the optimum amount of the $Fe_2O_3$ nanoparticles concentration was 0.5 wt% and the M3 membrane recorded the best performance among the prepared membrane series. Hence this membrane was subjected for the membrane re-usability studies and application on real water sample.

### 3.5. Membrane re-usability studies

Results of the membrane re-usability are presented in Fig. 8. It could be seen that the M3 membrane with 0.5 wt% $Fe_2O_3$ nanoparticles can be used up to 8 cycles without much loss in the fluoride removal efficiency. Sodium hydroxide was used as the neutralizing agent to desorb the fluoride ion from the iron oxide composite membrane. The high affinity of fluoride ion for the polarized sodium ions in solution helps in easy removal of the adsorbed fluoride from the membrane [47]. After 8 sequential cycles of membrane regeneration, the fluoride removal of the M3 membrane was observed as 66.4%, which was 4% less as compared to fresh run. Further regeneration resulted in a severe decrease in the fluoride removal efficiency. It is to be noted that the permeate flux of the membrane had no appreciable change for the regeneration cycles and was almost constant for each run. Membrane re-usability studies confirmed the durability and the better antifouling ability of the prepared $Fe_2O_3$ nanoparticles composite membrane with almost constant fluoride removal efficiency up to eight runs.

### 3.6. Application on real water sample

Real water samples were collected from ground water sources in Ranipet, Ambur and Vaniyambadi regions of Vellore district in Tamil Nadu, India. As shown in Table 4, the concentration of fluoride ions collected from Ranipet, Ambur and Vaniyambadi were estimated to be 0.6, 1.3 and 1.7 mg $L^{-1}$ respectively. After subjecting the water samples to ultra filtration experiments, the fluoride ion concentration of all the three permeate samples were found to be reduced below the detection limit of the measuring electrode which is 0.02 mg $L^{-1}$. To study the ability of the membrane to remove higher fluoride concentrations, the real water samples were spiked with 20 mg $L^{-1}$ of fluoride ions and percentage of fluoride removal obtained is reported in Table 5, for one run through the M3 membrane. A slight decrease in fluoride removal with the spiked real water samples was observed due to trivial interferences present in the water sample along with the fluoride ions. Continuous treatment of the feed stream through advanced membrane modules can produce a higher fluoride rejection for the reported membrane material and would bring the fluoride levels within the safe limits.

Table 4
Fluoride removal performance by 0.5 % $Fe_2O_3$ nanoparticles modified PES/CA blend membranes from unspiked real water samples

| Sampling site | Fluoride concentration in the sample (mg/L) | Fluoride concentration in the permeate (mg/L) | % of fluoride removed# |
|---|---|---|---|
| Ranipet | 0.6 | BDL* | > 96.7 |
| Ambur | 1.3 | BDL* | > 98.5 |
| Vaniyambadi | 1.7 | BDL* | > 98.8 |

*BDL – Below Detection Limit# - For a permeate concentration of 0.02 mg $L^{-1}$

## 4. Conclusion

Flat sheet membranes were prepared by addition of varying amounts of $Fe_2O_3$ nanoparticles to fixed amounts

Table 5
Fluoride removal performance by 0.5 % $Fe_2O_3$ nanoparticles modified PES/CA blend membranes from fluoride spiked real water samples

| Sampling site | Spiked fluoride concentration (mg/L) | Initial fluoride concentration (mg/L) | Final fluoride concentration (mg/L) | % of fluoride removed |
|---|---|---|---|---|
| Ranipet | 20 | 20.7 | 6.8 | 67.1 |
| Ambur | 20 | 21.2 | 7.3 | 65.6 |
| Vaniyambadi | 20 | 21.7 | 7.9 | 63.6 |

of polyether sulfone (PES) and cellulose acetate (CA). Prepared membranes were studied for their morphological and ultra filtration characteristics. $Fe_2O_3$ nanoparticles modified PES/CA membranes possessed improved hydrophilicity, enhanced porosity, lower membrane resistance, increased pore size and better water flux than the pristine PES and unmodified PES/CA blend membrane. $Fe_2O_3$ incorporated membranes showed a water flux nearly ten times higher as compared to the unmodified membranes. Fluoride removal studies revealed the potential of the synthesized iron oxide composite membrane as a strong defluoridation membrane. Adsorption was identified as the separation principle for the fluoride removal. Membrane with better fluoride rejection characteristics was obtained for 18 wt% PES, 2 wt% CA and 0.5 wt% $Fe_2O_3$ nanoparticles. This membrane possessed the maximum pure water flux of 156 L $m^{-2}$ $h^{-1}$ and highest fluoride removal efficiency of 70.3%. Re-usability studies of the 0.5 wt% $Fe_2O_3$ nanoparticles membrane for 8 cycles with almost constant rejection rate confirmed the longer durability of the composite membrane. Application of the membrane on fluoride spiked and unspiked real water samples using lab scale ultra filtration setup proved that the membrane was able to efficiently remove fluoride ions. A techno-economic study including detailed analysis of membrane fouling along with the fluoride adsorption and necessary mass transport modeling for the prepared PES/CA/$Fe_2O_3$ membrane material system can be performed as a future study.

## References


[1] N. Viswanathan, C.S. Sundaram, S. Meenakshi, Development of multi-functional chitosan beads for fluoride removal, J. Hazard. Mater., 167 (2009) 325–331.
[2] K. Singh, D.H. Lataye, K.L. Wasewar, C.K. Yoo, Removal of fluoride from aqueous solution: status and techniques, Desal. Water Treat., 51 (2013) 3233–3247.
[3] H. Strathmann, Membrane separation processes, J. Membr. Sci., 9 (1981) 121–189.
[4] A. Salahi, T. Mohammadi, A. Rahmat Pour, F. Rekabdar, Oily wastewater treatment using ultra filtration, Desal. Water Treat., 6 (2009) 289–298.
[5] M.N. Sarbolouki, A general diagram for estimating pore size of ultra filtration and reverse osmosis membranes, Sep. Sci. Technol., 17 (1982) 381–386.
[6] M. Cheryan, Ultra filtration and micro filtration handbook, Technomic Publishing Company Inc., Pennsylvania, 1998.
[7] A. Crull, Membranes for the nineties: Highlighting Surface Modification Technology, Business Communications Co., Norwalk, CT, 1990.
[8] J.F. Li, Z.L. Xu, H. Yang, Micro porous polyether sulfone membranes prepared under the combined precipitation conditions with non-solvent additives, Polym. Advan. Technol., 19 (2008) 251–257.
[9] H. Yu, Y. Zhang, J. Zhang, H. Zhang, J. Liu, Preparation and antibacterial property of $SiO_2$–Ag/PES hybrid ultra filtration membranes, Desal. Water Treat., 51 (2013) 3584–3590.
[10] W.J. Lau, A.F. Ismail, N. Misdan, M.A. Kassim, A recent progress in thin film composite membrane: a review, Desalination, 287 (2012) 190–199.
[11] N.A. Ali, S.S.M. Tari, Surface modification of polyethersulfone ultra filtration (PES-UF) membrane using myoglobin as modifying agent, Desal. Water Treat., 47 (2012) 171–181.
[12] G. Arthanareeswaran, P. Thanikaivelan, M. Raajenthiren, Fabrication and characterization of CA/PSf/SPEEK ternary blend ultra filtration membranes, Ind. Eng. Chem. Res., 47 (2008) 1488–1494.
[13] G. Arthanareeswaran, P. Thanikaivelan, K. Srinivasan, D. Mohan, M. Rajendran, Synthesis, characterization and thermal studies on cellulose acetate membranes with additive, Eur. Polym. J., 40 (2004) 2153–2159.
[14] G. Arthanareeswaran, K. Srinivasan, R. Mahendran, D. Mohan, M. Rajendran, V. Mohan, Studies on cellulose acetate and sulfonated poly(ether ether ketone) blend ultr afiltration membranes, Eur. Polym. J., 40 (2004) 751–762.
[15] S.A. Ahmed, M.H. Sorour, H.A. Talaat, S.S. Ali, Functional analysis of cellulose acetate flat membranes prepared via casting technique, Desal. Water Treat., 21 (2010) 115–121.
[16] A. Ghaee, M. Shariaty-Niassar, J. Barzin, T. Matsuura, A.F. Ismail, Preparation of chitosan/cellulose acetate composite nanofiltration membrane for wastewater treatment, Desal. Water Treat., 57 (2016) 14453–14460.
[17] G. Schmidt, M.M. Malwitz, Properties of polymer-nanoparticle composites, Curr. Opin. Colloid Interface Sci., 8 (2003) 103–108.
[18] G.R. Guillen, Y. Pan, M. Li, E.M. Hoek, Preparation and characterization of membranes formed by nonsolvent induced phase separation: a review, Ind. Eng. Chem., 50 (2011) 3798–3817.
[19] M. Homayoonfal, M.R. Mehrnia, Y.M. Mojtahedi, A.F. Ismail, Effect of metal and metal oxide nanoparticle impregnation route on structure and liquid filtration performance of polymeric nanocomposite membranes: a comprehensive review, Desal. Water Treat., 51 (2013) 3295–3316.
[20] J. Kim, B. Van der Bruggen, The use of nanoparticles in polymeric and ceramic membrane structures: review of manufacturing procedures and performance improvement for water treatment, Environ. Pollut., 158 (2010)2335–2349.
[21] S. Balta, A. Sotto, P. Luis, L. Benea, B. Van der Bruggen, J. Kim, A new outlook on membrane enhancement with nanoparticles: the alternative of ZnO, J. Membr. Sci., 389 (2012) 155–161.
[22] E. Bet-Moushoul, Y. Mansourpanah, K. Farhadi, M. Tabatabaei, $TiO_2$ nanocomposite based polymeric membranes: a review on performance improvement for various applications in chemical engineering processes, Chem. Eng. J., 283 (2016) 29–46.
[23] Q.F. Alsalhy, J.M. Ali, A.A. Abbas, A. Rashed, B. Van der Bruggen, S. Balta, Enhancement of poly (phenyl sulfone) membranes with ZnO nanoparticles, Desal. Water Treat., 51 (2013) 6070–6081.
[24] H.L. Richards, P.G. Baker, E. Iwuoha, Metal nanoparticle modified polysulfone membranes for use in wastewater treatment: a critical review, J. Surf. Eng. Mat. Adv. Tech., 2 (2012) 183–193.
[25] R. Saranya, G. Arthanareeswaran, A. F.Ismail, Dion D Dionysiou, D. Paul, Zero-valent iron impregnated mixed matrix

membranes for the treatment of textile effluent, RSC Adv., 5 (2015) 62486–62497.
[26] P.N. Dave, L.V. Chopd, Application of iron oxide nanomaterials for the removal of heavy metals, J. Nano. Tech., 2014 (2014) 1–14.
[27] P. Sabbatini, F. Yrazu, F. Rossi, G. Thern, A. Marajofsky, M.M. Fidalgo deCortalezzi, Fabrication and characterization of iron oxide ceramic membranes for arsenic removal, Water Res., 44 (2010) 5702–5712.
[28] H. Park, H. Choi, As(III) removal by hybrid reactive membrane process combined with ozonation, Water Res., 45 (2011) 1933–1940.
[29] P. Daraei, S.S. Madaeni, N. Ghaemi, E. Salehi, M.A. Khadivi, R. Moradian, B. Astinchap, Novel polyethersulfone nanocomposite membrane prepared by PANI/$Fe_3O_4$ nanoparticles with enhanced performance for Cu(II) removal from water, J. Membr. Sci., 415 (2012) 250–259.
[30] L.Y. Ng, A.W. Mohammad, C.P. Leo, N. Hilal, Polymeric membranes incorporated with metal/metal oxide nanoparticles: a comprehensive review, Desalination, 308 (2013) 15–33.
[31] A. Gholami, A.R. Moghadassi, S.M. Hosseini, S. Shabani, F. Gholami, Preparation and characterization of polyvinyl chloride based nanocomposite nanofiltration-membrane modified by iron oxide nanoparticles for lead removal from water, J. Ind. Eng. Chem., 20 (2014) 1517–1522.
[32] N.A. Weerasekara, K.H. Choo, S.J. Choi, Metal oxide enhanced micro filtration for the selective removal of Co and Sr ions from nuclear laundry wastewater, J. Membr. Sci., 447 (2013) 87–95
[33] X. Dou, Y. Zhang, H. Wang, T. Wang, Y. Wang, Performance of granular zirconium–iron oxide in the removal of fluoride from drinking water, Water Res., 45 (2011) 3571–3578.
[34] N. Chen, Z. Zhang, C. Feng, D. Zhu, Y. Yang, N. Sugiura, Preparation and characterization of porous granular ceramic containing dispersed aluminum and iron oxides as adsorbents for fluoride removal from aqueous solution, J. Hazard. Mater., 186 (2011) 863–868.
[35] E. Christina, P. Viswanathan, Development of a novel nano-biosorbent for the removal of fluoride from water, Chin. J. Chem. Eng., 23 (2015) 924–933.
[36] K. Nath, Membrane separation processes, PHI Learning Pvt. Ltd., New Delhi, 2008.
[37] R. Krishnamoorthy, V. Sagadevan, Polyethylene glycol and iron oxide nanoparticles blended polyethersulfone ultra filtration membrane for enhanced performance in dye removal studies, e-Polymers, 15 (2015) 151–159.
[38] S. Aditya Kiran, Y. Lukka Thuyavan, G. Arthanareeswaran, T. Matsuura, A.F. Ismail, Impact of graphene oxide embedded polyethersulfone membranes for the effective treatment of distillery effluent, Chem. Eng. J., 286 (2016) 528–537.
[39] Y. Lukka Thuyavan, N. Anantharaman, G. Arthanareeswaran, A.F. Ismail, Modification of polyethersulfone using sericin and polyvinylpyrrolidone for cadmium ion removal by polyelectrolyte- enhanced ultra filtration, Desal. Water Treat., 56 (2015) 366–378.
[40] K.I. Moideen, A.M. Isloor, A.F. Ismail, A. Obaid, H.K. Fun, Fabrication and characterization of new PSF/PPSU UF blend membrane for heavy metal rejection, Desal. Water Treat., 57 (2016) 19810–19819.
[41] V. Vatanpour, S.S. Madaeni, R. Moradian, S. Zinadini, B. Astinchap, Novel anti-fouling nanofiltration polyethersulfone membrane fabricated from embedding $TiO_2$ coated multi walled carbon nanotubes, Sep. Purif. Technol., 90 (2005) 69–82.
[42] A. Rahimpour, S.S. Madaeni, Polyethersulfone (PES)/cellulose acetate phthalate (CAP) blend ultra filtration membranes: preparation, morphology, performance and antifouling properties, J. Membr. Sci., 305 (2007) 299–312.
[43] J.F. Li, Z.L. Xu, H. Yang, L.Y. Yu, M. Liu, Effect of $TiO_2$ nanoparticles on the surface morphology and performance of micro porous PES membrane, Appl. Surf. Sci., 255 (2009) 4725–4732
[44] N.A.A. Hamid, A.F. Ismail, T. Matsuura, A.W. Zularisam, W.J. Lau, E. Yuliwati, M.S. Abdullah, Morphological and separation performance study of polysulfone/titanium dioxide (PSF/$TiO_2$) ultra filtration membranes for humic acid removal, Desalination, 273 (2011) 85–92.
[45] D. Maity, D.C. Agrawal, Synthesis of iron oxide nanoparticles under oxidizing environment and their stabilization in aqueous and non-aqueous media, J. Magn. Magn. Mater., 308 (2007) 46–55.
[46] V. Vatanpour, S.S. Madaeni, A.R. Khataee, E. Salehi, S. Zinadini, H.A. Monfared, $TiO_2$ embedded mixed matrix PES nanocomposite membranes: Influence of different sizes and types of nanoparticles on antifouling and performance, Desalination, 292 (2012) 19–29.
[47] S.M. Prabhu, S.S. Elanchezhiyan, G. Lee, S. Meenakshi, Defluoridation of water by graphene oxide supported needle-like complex adsorbents, J. In org. Organomet. P., 26 (2016) 834–844.